Approximated lax pairs and empirical interpolation for nonlinear parabolic partial differential equations

Jean-Frédéric Gerbeau, Damiano Lombardi, Elisa Schenone

APPROXIMATED LAX PAIRS AND EMPIRICAL INTERPOLATION FOR NONLINEAR PARABOLIC PARTIAL DIFFERENTIAL EQUATIONS

JEAN-FRÉDÉRIC GERBEAU*† DAMIANO LOMBARDI*† ELISA SCHENONE*†

1. Introduction. Several methods exist to approximate the solutions of PDEs with a reduced number of degrees of freedom (Reduced Basis Methods, Proper Orthogonal Decomposition, *etc.*). But time-dependent problems dominated by transport or propagation phenomena remain a challenge for reduced-order modelling.

In [6], a new approach was proposed to approximate the nonlinear evolution partial differential equations. This method, called ALP, is based on approximations of generalized Lax pairs. Contrary to other reduced-order methods, it is not based on an off-line / on-line strategy, and the basis on which the solution is searched for evolves in time according to a dynamics specific to the problem. This algorithm was successfully used for various nonlinear problems, including the equations of cardiac electrophysiology [7], which exhibit front propagation. Two weaknesses of the original method were the limitation to polynomial nonlinearities and a complexity proportional to the power three of the number of modes. In this article, a new algorithm is proposed which does not suffer from these two shortcomings.

The ALP-EI method introduced in this work combines the idea of ALP, i.e. a time evolving basis which does not rely on a database, and the treatment of nonlinear terms using a selection of spatial points from an Empirical Interpolation technique in the same spirit as in [1, 3]. More specifically, the definition of the basis functions and of their time evolution does not change compared to the ALP method, but the functions and the operator used to solve the reduced order problem are evaluated on a finite set of points which is typically a small subset of the finite element nodes. As a consequence, the ALP-EI method is well-suited to non-polynomial nonlinearities, and much less expensive than the original ALP method.

2. The ALP-EI method. Let Ω be a bounded subset of $\mathbb{R}^d$, with $d = 1, 2$ or 3, and $T > 0$. We consider a parabolic nonlinear partial differential equation (PDE):

$$\left\{ \begin{array}{rcll} \dfrac{\partial u}{\partial t} - \Delta u & = & f(u), & \text{in } \Omega \times (0,T), \\ \dfrac{\partial u}{\partial n} & = & 0, & \text{on } \partial\Omega \times (0,T), \\ u(0) & = & u_0, & \text{in } \Omega. \end{array} \right. \tag{2.1}$$

The nonlinear function f and the initial data u_0 are assumed to have a regularity sufficient to give a sense to all the formal computations hereafter.

2.1. The ALP method in a nutshell. In this Section, we briefly recall the main ideas of the Approximated Lax Pair (ALP) method proposed in [6]. In the ALP algorithm, the solution of the PDE (2.1) is approximated by an expansion on a time dependent basis:

$$u(x,t) \simeq \sum_{i=1}^{N_M} \beta_i(t) \varphi_i(x,t). \tag{2.2}$$

*Inria, 2 rue simone Iff, 75012 Paris, France.
†Sorbonne Universités UPMC, UMR 7598 LJLL, 75005 Paris, France.

The basis is made of eigenmodes defined by:

$$\mathcal{L}(u(x,t))\varphi_i(x,t) = \lambda_i(t)\varphi_i(x,t), \tag{2.3}$$

where $\mathcal{L}(u)$ is a linear Schrödinger operator:

$$\mathcal{L}(u)\varphi := -\Delta\varphi - \chi\, u\, \varphi, \tag{2.4}$$

where χ is a given positive parameter. The eigenmodes are solutions of an evolution equations:

$$\partial_t \varphi_i = \mathcal{M}(u)\varphi_i. \tag{2.5}$$

The ALP method relies on the observation that, in many situations, the solution u can be economically represented with a few modes defined by (2.3). If an approximation of (2.5) is available, then the eigenvalue problem has to be solved only once, and the modes can be propagated in time.

For some problems, like the Korteweg - de Vries equation, a closed form of $\mathcal{M}(u)$ can be obtained such that the Lax equation

$$\partial_t \mathcal{L}(u) + \mathcal{L}(u)\mathcal{M}(u) - \mathcal{M}(u)\mathcal{L}(u) = 0 \tag{2.6}$$

is satisfied when u is solution to (2.1). In such a case, the eigenvalues λ_i have the remarkable property to be constant in time, which provides first integrals of the dynamics, and the operators $\mathcal{L}(u)$ and $\mathcal{M}(u)$ are known as Lax pairs [9]. In general, the closed form of $\mathcal{M}(u)$ is unknown and/or the eigenvalues are not constant. In these cases, approximations of $\mathcal{M}(u)$ and of the equation satisfied by the eigenvalues were proposed in [6]. The approximation was based on a L^2 projection of the equations on the eigenmodes. To avoid the shortcomings recalled in the introduction, we propose another strategy in the following.

2.2. Finite element formulation of the Approximated Lax Pair. From now, the "full-order model" refers to the approximation of (2.1) on a finite dimensional space V constructed with continuous piecewise affine functions. The quantities $\varphi, u, \mathcal{L}, \mathcal{M}, \dots$ used in the previous section now denote their finite element counterpart. The finite element basis of V is denoted by $(v_1, \dots, v_{\mathcal{N}})$. The solution $u(x,t) = \sum_{i=1}^{\mathcal{N}} u_i(t)v_i(x) \in V$ of the full-order model is such that for $i = 1, \dots, \mathcal{N}$,

$$\int_\Omega \partial_t u v_i + \int_\Omega \nabla u \cdot \nabla v_i = \int_\Omega f(u)v_i. \tag{2.7}$$

The finite element approximation of the eigenmodes of (2.3) is given by:

$$\varphi_k(x,t) = \sum_{j=1}^{\mathcal{N}} \Phi_{jk}(t)v_j(x), \qquad \text{for } k = 1, \dots, N_M.$$

The vector $\Phi_k(t) \in \mathbb{R}^{\mathcal{N}}$ denotes the components of $\varphi_k(x,t)$ on the finite element basis: $\Phi_k(t) = (\Phi_{jk}(t))_{j=1\dots\mathcal{N}}$. The following $\mathcal{N} \times \mathcal{N}$ matrices are defined:

$$\mathcal{L}(u) = \left[\int_\Omega \nabla v_j \cdot \nabla v_i - \chi \int_\Omega u v_j v_i]\right]_{i,j=1\dots\mathcal{N}}, \quad \partial_t \mathcal{L}(u) = \left[-\chi \int_\Omega \partial_t u v_j v_i\right]_{i,j=1\dots\mathcal{N}},$$

and the Gram (or mass) matrix $\mathcal{G} = \left[\int_\Omega v_j v_i\right]_{i,j=1\dots\mathcal{N}}$.

The usual Euclidian scalar product in $\mathbb{R}^{\mathcal{N}}$ is denoted by $\langle\cdot,\cdot\rangle$. Another scalar product is defined in $\mathbb{R}^{\mathcal{N}}$ by $\langle\cdot,\cdot\rangle_{\mathcal{G}} = \langle\mathcal{G}\cdot,\cdot\rangle$. With this notation, $\int_\Omega \varphi_k\varphi_l = \langle\Phi_k,\Phi_l\rangle_{\mathcal{G}}$.

The vectors $\Phi_k(t)$ satisfy

$$\mathcal{L}(u(t))\Phi_k(t) = \lambda_k(t)\mathcal{G}\Phi_k(t), \tag{2.8}$$

and are normalized such that $\langle\Phi_k,\Phi_l\rangle_{\mathcal{G}} = \delta_{kl}$, where δ_{kl} is the Kronecker delta.

Let M be the $N_M \times N_M$ skew-symmetric matrix M defined by:

$$M_{kl} = \langle\partial_t\Phi_l,\Phi_k\rangle_{\mathcal{G}}. \tag{2.9}$$

PROPOSITION 2.1. *Let u be the solution of (2.7). Let $\Phi_k(t)$ be the eigenmodes and $\lambda_k(t)$ the eigenvalues defined by (2.8). Then*

$$\partial_t\lambda_k = -\chi\int_\Omega \partial_t u\varphi_k^2. \tag{2.10}$$

Let M be the matrix defined by (2.9). If k and l are such that $\lambda_k \neq \lambda_l$, then

$$M_{kl} = \frac{\chi}{\lambda_k-\lambda_l}\int_\Omega \partial_t u\varphi_k\varphi_l. \tag{2.11}$$

Proof. The time derivative of (2.8) gives:

$$\partial_t\mathcal{L}(u)\Phi_k + (\mathcal{L}(u)-\lambda_k\mathcal{G})\partial_t\Phi_k = \partial_t\lambda_k\mathcal{G}\Phi_k \tag{2.12}$$

Taking the scalar product with Φ_l and using the symmetry of the matrix $\mathcal{L}(u)$,

$$\langle\partial_t\mathcal{L}(u)\Phi_k,\Phi_l\rangle + (\lambda_l-\lambda_k)\langle\mathcal{G}\partial_t\Phi_k,\Phi_l\rangle = \partial_t\lambda_k\langle\mathcal{G}\Phi_k,\Phi_l\rangle,$$

Thus

$$(\lambda_l-\lambda_k)M_{lk} = \partial_t\lambda_k\delta_{kl} + \chi\int_\Omega \partial_t u\varphi_k\varphi_l,$$

hence the result. □

Remark 2.1. *Denoting by $\mathcal{M}(u)$ the matrix such that $\partial_t\Phi_k = \mathcal{M}(u)\Phi_k$, relation (2.12) reads:*

$$\partial_t\mathcal{L}(u)\Phi_k + \mathcal{L}(u)\mathcal{M}(u)\Phi_k - \mathcal{M}(u)\mathcal{L}(u)\Phi_k = \partial_t\lambda_k\Phi_k$$

which is a discrete counterpart of the Lax equation (2.6) in the non-isospectral case. But the matrix $\mathcal{M}(u)$ being not explicitly known, this relation is of no practical use in this form. Matrix M defined by (2.9) can be viewed as an approximation of $\mathcal{M}(u)$ since $M_{kl} = \langle\mathcal{M}(u)\Phi_l,\Phi_k\rangle_{\mathcal{G}}$.

Remark 2.2. *Consider the equation:*

$$(\lambda_l-\lambda_k)M_{lk} = \partial_t\lambda_k\delta_{kl} + \chi\int_\Omega \partial_t u\varphi_k\varphi_l,$$

When $l \neq k$, but $\lambda_l = \lambda_k$, i.e. *when there is a degenerate eigenvalue (multiplicity greater than one), there is an orthogonal transformation invariant subspace spanned by the corresponding eigenfunctions, and the equation for M_{lk} does no longer make sense. The resolution of this degeneracy is a classical result in the perturbation theory in quantum mechanics. In particular, when $\lambda_l = \lambda_k$, the evolution representation reads: $\langle \partial_t \varphi_l, \varphi_k \rangle = 0$. The fact that the eigenfunctions are defined up to a transformation can be used to solve this equation. Let us consider the sub-matrix whose entries are $S_{ij} = \langle \partial_t u \varphi_l, \varphi_k \rangle$, for the indices corresponding to $\lambda_l = \lambda_k$. The eigenvectors of S define a linear combination of the eigenfunctions such that the evolution operator representation is zero. When using this linear combination to update the eigenfunction, we obtain that the eigenvalue crossing results in a "jump" of the eigenfunctions.*

Remark 2.3. *In the original ALP method, $\partial_t u$ was approximated by an expansion $\sum_{i=1}^{N_M} \gamma_i \varphi_i$ and the quantity $\int_\Omega \partial_t u \varphi_k \varphi_l$ in (2.10) and (2.11) was approximated by $\sum_{i=1}^{N_M} \gamma_i \int_\Omega \varphi_i \varphi_k \varphi_l$. The third order tensor $[\int_\Omega \varphi_i \varphi_k \varphi_l]$ had to be propagated (see Section 3.3 of [6]), which could be costly when the number of mode N_M was high. Besides, to relate the components γ_i of $\partial_t u$ to the components β_i of u, the nonlinearity of $f(u)$ was supposed to be polynomial.*

2.3. Approximation of the finite element formulation. In this section we derive an approximation of the quantity $\int_\Omega \partial_t u \varphi_k \varphi_l$, which appears in the expression of (2.10) and (2.11). For $k = 1, \ldots, N_M$, the evolution of the eigenvector Φ_k is approximated by:

$$\partial_t \tilde{\Phi}_k = \tilde{M} \tilde{\Phi}_k. \tag{2.13}$$

where $\tilde{M}$ will be defined below. An approximation $\tilde{U}(t) \in \mathbb{R}^{\mathcal{N}}$ of the degrees of freedom of the solution $u(\cdot, t) \in V$ is searched for as an expansion on the eigenvectors:

$$\tilde{U}(t) = \sum_{l=1}^{N_M} \beta_l(t) \tilde{\Phi}_l(t). \tag{2.14}$$

Thus we have:

$$\partial_t \tilde{U} = \sum_{l=1}^{N_M} \partial_t \beta_l \tilde{\Phi}_l + \sum_{l=1}^{N_M} \beta_l \tilde{M} \tilde{\Phi}_l,$$

and by projection on $\tilde{\Phi}_k$, we obtain:

$$\partial_t \beta_k + \sum_{l=1}^{N_M} \tilde{M}_{kl} \beta_l = \langle \partial_t \tilde{U}, \tilde{\Phi}_k \rangle_{\mathcal{G}}. \tag{2.15}$$

For any continuous fonction g defined on Ω, we will use the following approximation repeatedly :

$$\int_\Omega g v_i \simeq \sum_{j=1}^{\mathcal{N}} \left(\int_\Omega v_j v_i \right) g_j, \tag{2.16}$$

where g_j denotes the interpolation of g at the j-th finite element nodes.

Multiplying (2.8) by β_k and summing over k, we obtain:

$$\mathcal{L}(u(t))\tilde{U}(t) = \sum_{k=1}^{N_M} \lambda_k(t)\beta_k(t)\mathcal{G}\tilde{\Phi}_k(t),$$

thus

$$K\tilde{U} = \chi \left[\int_\Omega u v_j v_i \right]_{i,j} \tilde{U} + \sum_{k=1}^{N_M} \lambda_k \beta_k \mathcal{G}\tilde{\Phi}_k.$$

With the approximation (2.14) and (2.16), we have:

$$K\tilde{U} \simeq \chi \mathcal{G}(\tilde{U} \odot \tilde{U}) + \sum_{k=1}^{N_M} \lambda_k \beta_k \mathcal{G}\tilde{\Phi}_k,$$

where $\odot$ denotes the Hadamard product, i.e. the element-by-element multiplication. Then using this approximation in (2.7), and again (2.14) and (2.16), we obtain:

$$\mathcal{G}\partial_t\tilde{U} + \chi\mathcal{G}(\tilde{U} \odot \tilde{U}) + \sum_{k=1}^{N_M} \lambda_k \beta_k \mathcal{G}\tilde{\Phi}_k \simeq \mathcal{G}f(\tilde{U}),$$

where $f(\tilde{U})$ denotes the vector $(f(\tilde{U}_j))_{j=1\dots\mathcal{N}}$. We therefore obtain the following approximation

$$\partial_t\tilde{U} \simeq f(\tilde{U}) - \chi\tilde{U} \odot \tilde{U} - \sum_{k=1}^{N_M} \lambda_k \beta_k \tilde{\Phi}_k. \tag{2.17}$$

Using (2.14), we have:

$$\int_\Omega \partial_t u \varphi_k \varphi_l \simeq \sum_{j=1}^{\mathcal{N}} \left(\int_\Omega v_j \varphi_l \right) \partial_t \tilde{U}_j \tilde{\Phi}_{jk} = \sum_{i,j=1}^{\mathcal{N}} \Phi_{il} \left(\int_\Omega v_j v_i \right) \partial_t \tilde{U}_j \tilde{\Phi}_{jk}.$$

Combining the last two expressions, we obtain the following approximation:

$$\int_\Omega \partial_t u \varphi_k \varphi_l \simeq \tilde{\Phi}_l^T \mathcal{G}(\tilde{\Phi}_k \odot \tilde{F}), \tag{2.18}$$

where $\tilde{F} = f(\tilde{U}) - \chi\tilde{U} \odot \tilde{U} - \sum_{k=1}^{N_M} \lambda_k \beta_k \tilde{\Phi}_k$.

Thus, we deduce from (2.10) and (2.11):

$$\partial_t \lambda_k = -\chi \int_\Omega \partial_t u \varphi_k^2 \approx -\chi \tilde{\Phi}_k^T \mathcal{G}(\tilde{\Phi}_k \odot \tilde{F}), \tag{2.19}$$

$$M_{kl} = \frac{\chi}{\lambda_k - \lambda_l} \int_\Omega \partial_t u \varphi_k \varphi_l \approx \frac{\chi}{\lambda_k - \lambda_l} \tilde{\Phi}_l^T \mathcal{G}(\tilde{\Phi}_k \odot \tilde{F}). \tag{2.20}$$

2.4. The ALP-EI algorithm. In the previous section, we derived the approximation (2.18), which can be used to approximate the expression (2.11) of the operator M, and the differential equation (2.10) satisfied by the eigenvalues λ_k. But in (2.18), the size of the vectors is the dimension $\mathcal{N}$ of the full order space. To obtain a reduced order model, we have to further simplify this expression. To do so, we introduce N_P interpolation points, which are picked among the $\mathcal{N}$ nodes of the finite element mesh. The choice of these points will be explained in Section 2.6. Consider the interpolation matrix

$$P = \left[e_{p_1}, \dots, e_{p_{N_P}}\right] \in \mathbb{R}^{\mathcal{N}, N_P},$$

where $e_{p_j} = [0, \dots, 0, 1, 0, \dots, 0]^T \in \mathbb{R}^{\mathcal{N}}$ is the p_i-th column of the identity matrix of $\mathbb{R}^{\mathcal{N}\times\mathcal{N}}$. For $k = 1 \dots N_P$, we define $\Phi_k(0) \in \mathbb{R}^{\mathcal{N}}$ as the first N_P normalized modes solution to problem (2.8), and the vectors $\Psi_k \in \mathbb{R}^{N_P}$ by

$$\Psi_k = P^T \Phi_k(0).$$

We denote by $\mathbf{\Phi}(0)$ the $\mathcal{N} \times N_P$ matrix whose columns are the vectors $\Phi_j(0)$, $j = 1 \dots N_P$, by $\mathbf{\Psi}$ the $N_P \times N_P$ matrix whose columns are the vectors Ψ_j, $j = 1 \dots N_P$, and by $\hat{\mathbf{\Phi}}(t)$ the $N_P \times N_M$ matrix whose columns are the $\hat{\Phi}_j(t)$, $j = 1 \dots N_M$ (see Fig. 2.1).

We recall that the basis $(\Phi_k(0))_{k=1\dots N_M}$ is orthonormal with respect to the scalar product $\langle \cdot, \cdot \rangle_{\mathcal{G}}$ defined by the Gram matrix $\mathcal{G}$. This is of course no longer true for the basis $(\Psi_k)_{k=1\dots N_M}$. We therefore introduce a new matrix $G \in \mathbb{R}^{N_P \times N_P}$ such that $(\Psi_k)_{k=1\dots N_M}$ is orthonormal for the scalar product $\langle \cdot, \cdot \rangle_G$, i.e. $\mathbf{\Psi}^T G \mathbf{\Psi} = I$, where $I \in \mathbb{R}^{N_P \times N_P}$ is the identity matrix. The matrix $\mathbf{\Psi}$ can be QR-decomposed $\mathbf{\Psi} = QR$, where Q is an orthonormal matrix and R is an upper triangular matrix, which is obtained without any extra costs when applying a modified Gram-Schmidt orthonormalization. Then, the expression of G can be obtained, offline and once for all, by

$$G = QR^{-T}R^{-1}Q^T. \tag{2.21}$$

Then we can repeat *mutatis mutandis* the derivation presented in the previous Section, the only change being that the Gram matrix $\mathcal{G}$ is replaced by G. The interpolation $\hat{U}(t)$ of the solution $u(\cdot, t) \in V$ is now searched for in the space $\mathbb{R}^{N_P}$ and its expansion on the mobile basis $(\hat{\Phi}_l(t))_{l=1\dots N_M}$ is given by:

$$\hat{U}(t) = \sum_{l=1}^{N_M} \hat{\beta}_l(t) \hat{\Phi}_l(t). \tag{2.22}$$

The counterpart of (2.15) is

$$\partial_t \hat{\beta}_k + \sum_{l=1}^{N_M} \hat{M}_{kl} \hat{\beta}_l = \langle \partial_t \hat{U}, \hat{\Phi}_k \rangle_G.$$

The counterpart of (2.17) is

$$\partial_t \hat{U} = f(\hat{U}) - \chi \hat{U} \odot \hat{U} - \sum_{l=1}^{N_M} \hat{\lambda}_l \hat{\beta}_l \hat{\Phi}_l := \hat{F}$$

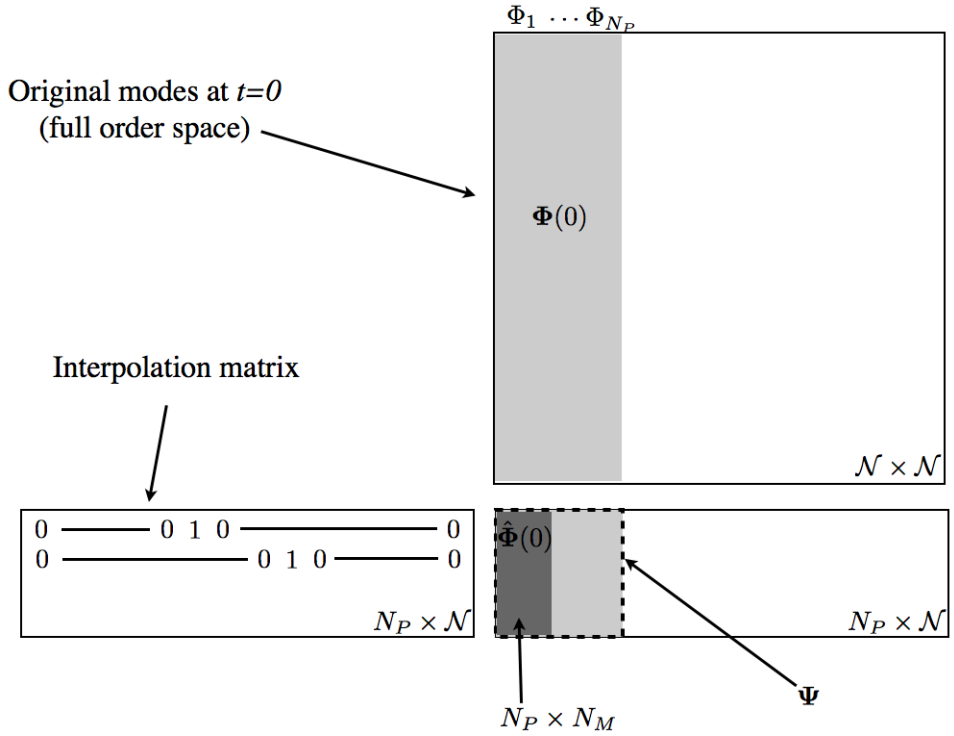

FIG. 2.1. *Schematic representation of matrices* $\mathbf{\Phi}(0)$, $\mathbf{\Psi}$ *and* $\hat{\mathbf{\Phi}}(0)$.

And the counterparts of (2.18) and (2.19) are:

$$\partial_t \hat{\lambda}_k = -\chi \hat{\Phi}_k^T G(\hat{\Phi}_k \odot \hat{F}),$$

and

$$\hat{M}_{kl} = \frac{\chi}{\hat{\lambda}_k - \hat{\lambda}_l} \hat{\Phi}_l^T G(\hat{\Phi}_k \odot \hat{F}).$$

To summarize, for $k = 1 \dots N_M$, $\hat{\beta}_k(t)$ and $\hat{\Phi}_k(t)$ are defined by:

$$\left\{ \begin{array}{rcl} \partial_t \hat{\beta}_k + \sum_{l=1}^{N_M} \hat{M}_{kl} \hat{\beta}_l & = & \hat{F}^T G \hat{\Phi}_k, \\ \partial_t \hat{\Phi}_k & = & \hat{M} \hat{\Phi}_k, \\ \partial_t \hat{\lambda}_k & = & -\chi \hat{\theta}_{kk}, \\ \hat{M}_{kl} & = & \frac{\chi}{\hat{\lambda}_k - \hat{\lambda}_l} \hat{\theta}_{kl}, \text{ if } \hat{\lambda}_k \neq \hat{\lambda}_l, \text{ and } \hat{M}_{kl} = 0 \text{ if } \hat{\lambda}_k = \hat{\lambda}_l, \\ \hat{\theta}_{kl} & = & \hat{\Phi}_l^T G(\hat{\Phi}_k \odot \hat{F}), \\ \hat{F} & = & f(\hat{U}) - \chi \hat{U} \odot \hat{U} - \sum_{l=1}^{N_M} \hat{\lambda}_l \hat{\beta}_l \hat{\Phi}_l. \end{array} \right. \tag{2.23}$$

2.5. Reconstruction in the full order space. The solution (2.22) obtained with the ALP-EI algorithm (2.23) only involves computations in the reduced order space. We now explain how the solution can be reconstructed in the full order space. This reconstruction is simplified with respect to the original version of ALP. This is possible because in ALP-EI we make use of an intermediate space whose basis is the initial basis of size N_{P}. Whatever the evolution of the N_{M} modes is, it can be described exactly in this extended initial basis, which is in a bijection with the collocation basis on the N_{P} points.

PROPOSITION 2.2. *The coordinates $c(t) \in \mathbb{R}^{N_P}$ of $\hat{U}(t)$ on the basis $(\Psi_i)_{i=1\dots N_P}$ are given by*

$$c(t) = \boldsymbol{\Psi}^T G \hat{\boldsymbol{\Phi}}(t) \hat{\beta}(t). \tag{2.24}$$

Proof. The basis $(\Psi_i)_{i=1\dots N_P}$ being orthonormal for the scalar product induced by G, we have:

$$\hat{\Phi}_i(t) = \sum_{j=1}^{N_P} \langle \Psi_j, \hat{\Phi}_i(t) \rangle_G \Psi_j.$$

Thus:

$$\hat{U}(t) = \sum_{i=1}^{N_M} \hat{\beta}_i(t) \left(\sum_{j=1}^{N_P} \langle \Psi_j, \hat{\Phi}_i(t) \rangle_G \Psi_j \right) = \sum_{i=1}^{N_P} \left(\sum_{j=1}^{N_M} \langle \Psi_i, \hat{\Phi}_j(t) \rangle_G \hat{\beta}_j(t) \right) \Psi_i,$$

thus, $c_i = \sum_{j=1}^{N_M} \langle \Psi_i, \hat{\Phi}_j(t) \rangle_G \hat{\beta}_j(t)$. Hence the result since $\langle \Psi_i, \hat{\Phi}_j(t) \rangle_G$ is the entry (i,j) of the matrix $\boldsymbol{\Psi}^T G \hat{\boldsymbol{\Phi}}(t)$. ∎

Following the same approach as in DEIM [3], the solution in the full order space is obtained by keeping the same coordinates $c(t)$ in the basis $(\Phi_k(0))_{k=1\dots N_M}$, i.e. $u(t) \simeq \boldsymbol{\Phi}(0) c(t)$. Thus:

$$u(t) \simeq \boldsymbol{\Phi}(0) \boldsymbol{\Psi}^T G \hat{\boldsymbol{\Phi}}(t) \hat{\beta}(t).$$

Defining the $\mathcal{N} \times N_M$ matrix $\Pi = \boldsymbol{\Phi}(0) \boldsymbol{\Psi}^T G$, the reconstruction in the full order space of the reduced solution $\hat{U}(t)$ is given by:

$$u(t) \simeq \Pi \hat{U}(t) \tag{2.25}$$

Note that Π can be computed off-line once for all. The online cost of the reconstruction is therefore $\mathcal{N} \times N_{\mathrm{P}}$.

2.6. Choice of the interpolation points. We explain in this section the algorithm used to select the interpolation points. The set of the $\mathcal{N}$ vertices of the finite element mesh is denoted by Ω_p. Consider the set of N_P eigenmodes, which are represented by the columns of the matrix $\boldsymbol{\Phi}(0)$. The index of the first point is chosen such that $p_1 = \arg\max_{1 \le i \le \mathcal{N}} \Phi_{i1}(0)$. The objective is to define a greedy algorithm to select N_P points out of $\mathcal{N}$. Given a set of indices of points $\mathcal{P} = \{p_1, \dots, p_n\}$ the index of the $(n+1)$-th point will be chosen in $\Omega_p \backslash \mathcal{P}$.

When n points are known, with $n < N_p$, the matrix $\mathbf{\Psi}^{(n)} \in \mathbb{R}^{n\times n}$, whose entries are defined by $\Psi_{ij}^{(n)} := \Phi_{p_i j}(0)$, is the matrix whose $j-$th column is the set of the values of the $j-$th eigenfunction evaluated at the n points whose indices are in $\mathcal{P}$. Assume that the matrix $\mathbf{\Psi}^{(n)}$ is full rank, *i.e.* $\text{rank}(\mathbf{\Psi}^{(n)}) = n$. Define an augmented matrix $\tilde{\mathbf{\Psi}}^{(n)} \in \mathbb{R}^{n\times n+1}$ by appending a column with the values of the $(n+1)$-th eigenfunction evaluated at the n points with indices in $\mathcal{P}$: $\tilde{\mathbf{\Psi}}^{(n)} \in \mathbb{R}^{n\times n+1} = [\mathbf{\Psi}^{(n)}, \Psi_{p_1\dots p_n,n+1}]$, where $\Psi_{p_1\dots p_n,n+1}$ is a notation for the components $p_1,\dots,p_n$ of the vector Ψ_{n+1}. The rank of the augmented matrix $\tilde{\mathbf{\Psi}}^{(n)}$ is still n. The objective is to select a point of index $p_{n+1} \in \Omega_p\backslash\mathcal{P}$ in such a way that the vector $w := \Psi_{p_{n+1},1:n+1} \in \mathbb{R}^{1\times n+1}$ is "as orthogonal as possible" to the first n rows of $\tilde{\mathbf{\Psi}}^{(n)}$. More formally, denoting by w_j the vector $\Psi_{p_j,1:n+1}$, i.e. the values of the $n+1$ eigenfunctions evaluated in the candidate point p_j. For every candidate point p_j, the best least squares approximation of w_j in terms of the rows of the matrix $\tilde{\mathbf{\Psi}}^{(n)}$ is computed. The point p_{n+1} is the one for which the approximation is the worst. In other words:

$$p_{n+1} = \arg\max_{p_j\in\Omega_p\backslash\mathcal{P}} \|w_j - \sum_{i=1}^{n} \alpha_i(w_j)\tilde{\Psi}_{i,1:n+1}^{(n)}\|_2^2,$$

with

$$\alpha(w_j) = \arg\min_{\alpha\in\mathbb{R}^n} \|w_j - \sum_{i=1}^{n} \alpha_i\tilde{\Psi}_{i,1:n+1}^{(n)}\|_2^2.$$

Note that, $\tilde{\mathbf{\Psi}}^{(n)}$ being of rank n, the matrix $\tilde{\mathbf{\Psi}}^{(n)}(\tilde{\mathbf{\Psi}}^{(n)})^T \in \mathbb{R}^{n\times n}$ is symmetric positive definite. The normal equation associated with the least squares approximation of w_j is therefore well posed.

To conclude, note that necessarily $\|w_j - \sum_{i=1}^{n} \alpha_i(w_j)\tilde{\Psi}_{i,1:n+1}^{(n)}\|_2^2 > 0$ for at least one j, otherwise this would contradict the fact that the eigenmodes are linearly independent. Thus the rank of the matrix $\mathbf{\Psi}^{(n+1)} \in \mathbb{R}^{n+1\times n+1}$ is $n+1$, so that the hypothesis of full rank of this matrix at the subsequent iteration will be fulfilled. A pseudo-code of the method is presented in Algorithm 1. In Figure 2.2 we show an example of 50 points obtained for the Laplace operator modes on the mesh of a 2D square.

2.7. Error analysis: Lebesgue constant. In order to assess the interpolation error associated with the choice of the collocation points for the basis of the Schrödinger eigenfunctions, the Lebesgue constant (see [5, 11]) is investigated as a function of the number of collocation points. The analysis is performed in the spirit of the one proposed in [8] in the context of Reduced Basis methods. The Lebesgue constant is defined by:

$$\Lambda_{N_P} = \sup_{x\in\Omega} \sum_{m=1}^{N_P} |V_m^{N_P}(x)|, \tag{2.26}$$

where the $V_m^{N_P}(x) \in \mathbb{R}^M$ are characteristic functions satisfying $V_m^{N_P}(x_{p_n}) = \delta_{mn},\ 1 \leq n, m \leq N_P$. Let the interpolation error be denoted by $\epsilon_{N_P}(t)$ and the best approximation error by $\epsilon_{N_P}^*(t)$. It can be shown as in [8] that they satisfy $\epsilon_{N_P}(t) \leq \epsilon_{N_P}^*(t)(1+\Lambda_{N_P}), \forall t \geq 0$. It is therefore useful to have an idea of the behavior of the Lebesgue constant with respect to the number of collocation points to have an estimation of the interpolation error.

Algorithm 1 Choice of the interpolation points

Let $p_1 \in \Omega_p$ and $\mathbf{\Psi}^{(1)} = [\Phi_{p_1,1}]$
for $k = 1 : N_{\mathrm{P}} - 1$ **do**
  $\mathcal{J}^* = 0.$
  $p_{k+1} = 0.$
  for $j = 1 : \mathcal{N} - k$ **do**
    $w_j = [\Phi_{p_j,1} \cdots \Phi_{p_j,k+1}] \in \mathbb{R}^{k+1}$
    $\alpha^* = \arg\min_{\alpha} \|w_j - \sum_{i=1}^{k} \alpha_i \tilde{\Psi}_{i,1:k+1}\|_2^2$
    $\mathcal{J} = \|w_j - \sum_{i=1}^{k} \alpha_i^* \tilde{\Psi}_{i,1:k+1}\|_2^2$
    if $\mathcal{J} > \mathcal{J}^*$ **then**
      $\mathcal{J}^* = \mathcal{J}$
      $p_{k+1} = p_j$
    end if
  end for
  $\Psi^{(k+1)} \in \mathbb{R}^{k+1,k+1} = \Phi_{p_1 \dots p_{k+1},1:k+1}.$
end for
return $(p_1, \dots p_{N_P}), \Psi \in \mathbb{R}^{N_P \times N_P}$

$$\left(\begin{array}{c|c} & \Phi_{p_1,k+1} \\ \mathbf{\Psi}^{(k)} & \vdots \\ & \Phi_{p_k,k+1} \\ \hline \Phi_{p_{k+1},1} \dots & \Phi_{p_{k+1},k+1} \end{array}\right)$$

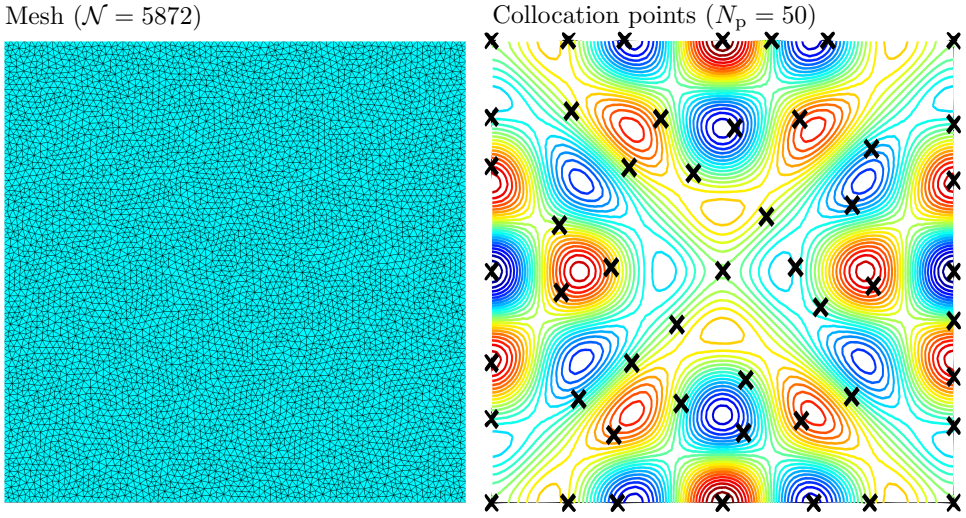

FIG. 2.2. *On the left a FE mesh, on the right the 50th Laplace mode (discretized on the FE mesh) and the correspondig 50 points found with Algorithm 1.*

In our procedure for the selection of the points, the values of the Lebesgue constant can be computed straightforwardly. The expansions of $V_m^{N_P}$ on the finite element basis $(v_j)_{j=1\dots\mathcal{N}}$ and on the eigenmodes $(\varphi_j(x,0))_{1\dots N_P}$ at $t = 0$ read

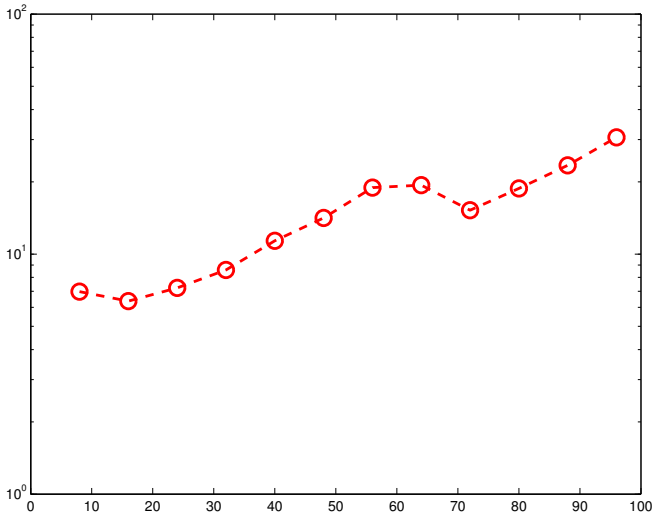

FIG. 2.3. *Lebesgue constant Λ_{N_P} as a function of N_P.*

$$V_m^{N_P}(x) = \sum_{j=1}^{\mathcal{N}} V_{jm} v_j(x) = \sum_{j=1}^{N_P} W_{jm} \varphi_j(x,0) = \sum_{j=1}^{\mathcal{N}} \sum_{i=1}^{N_P} \Phi_{ji}(0) W_{im} v_j(x),$$

thus $\mathbf{V}^{N_P} = \mathbf{\Phi}(0)\mathbf{W}$, where $\mathbf{V}^{N_P} = [V_{ij}] \in \mathbb{R}^{\mathcal{N} \times N_P}$ and $\mathbf{W} = [W_{ij}] \in \mathbb{R}^{N_P \times N_P}$. By noticing that

$$V_m^{N_P}(x_{p_n}) = \delta_{mn} = \sum_{j=1}^{N_P} W_{jm} \varphi_j(x_{p_n}, 0) = \sum_{j=1}^{N_P} W_{jm} \Psi_{nj},$$

we deduce that $\mathbf{W} = \mathbf{\Psi}^{-1}$. Thus:

$$\mathbf{V}^{N_P} = \mathbf{\Phi}(\mathbf{0})\mathbf{\Psi}^{-1}.$$

With Definition (2.26), it is therefore straightforward to deduce Λ_{N_P}. In Figure 2.3 we show the value of the Lebesgue constant varying the number of points. While theoretically it is difficult to obtain estimates which are sharper than a behavior in 2^{N_P}, we can see numerically that the Lebesgue constant grows approximately in a linear way.

3. Numerical results. In this section some numerical experiments are presented, on nonlinear reaction diffusion equations. All the test-cases presented are in 2D.

The first test case deals with the reduced integration of the Fisher-Kolmogorov-Petrovski-Piskunov equation (FKPP), for which the nonlinearity is polynomial. Then, several examples of monodomain equations used in electro-physiology are shown, for which the nonlinearity is non-polynomial.

3.1. FKPP. The FKPP equation reads:

$$\begin{cases} \dfrac{\partial u}{\partial t} - \Delta u = cu(1-u), & \Omega = [0,1]^2, \\ u = 0, & \partial\Omega. \end{cases} \tag{3.1}$$

The ALP-EI scheme is detailed for this equation, to provide a less abstract example of the discretisation. The solution u is approximated on the first N_M modes:

$$\sum_{i=1}^{N_M} \partial_t \beta_i \varphi_i + \beta_i \partial_t \varphi_i - \beta_i \Delta \varphi_i = cu(1-u). \tag{3.2}$$

The spectral problem is substituted:

$$-\Delta\varphi_i = \chi u \varphi_i + \lambda_i \varphi_i \;\Rightarrow \sum_{i=1}^{N_M} \partial_t \beta_i \varphi_i + \beta_i \partial_t \varphi_i + \beta_i \left(\chi u \varphi_i + \lambda_i \varphi_i\right) = cu(1-u). \tag{3.3}$$

After some algebra and by noticing that $\sum_i \beta_i u \varphi_i = u^2$, the expression becomes:

$$\sum_{i=1}^{N_M} \partial_t \beta_i \varphi_i + \beta_i \partial_t \varphi_i = cu(1-u) - \chi u^2 - \sum_{i=1}^{N_M} \beta_i \lambda_i \varphi_i. \tag{3.4}$$

This equation is discretised on the N_P points and the equations for the coefficients $\hat{\beta}$ is found by projecting the equation on the basis:

$$\partial_t \hat{\beta} + \hat{M}\hat{\beta} = (cI + \hat{\Lambda})\hat{\beta} - (c+\chi)\langle \hat{u}^2, \hat{\mathbf{\Phi}} \rangle. \tag{3.5}$$

Remark that this equation does not contain the discretisation of space differential operators, by virtue of the substitution of the spectral problem. The equation has been discretised by a mixed semi-implicit scheme of the form :

$$\left(\frac{I}{\Delta t} - \frac{c + \hat{\Lambda}^{(n)}}{2}\right)\hat{\beta}^{(n+1)} = \left(\frac{I}{\Delta t} + \frac{c + \hat{\Lambda}^{(n)}}{2}\right)\hat{\beta}^{(n)} - \hat{M}^{(n)}\hat{\beta}^{(n)} - (c+\chi)\langle \hat{u^{(n)}}^2, \hat{\mathbf{\Phi}} \rangle \tag{3.6}$$

The full-order problem is defined on the unitary square $\Omega = [0,1]^2$, discretised by a P_1 finite element, the number of degrees of freedom is $\mathcal{N} \approx 5\ 10^3$. The initial solution is $u_0 = g(\mu, \sigma^2)$ where g is a gaussian centered around $\mu = [0.25, 0.25]$ and $\sigma^2 = \mathrm{diag}[0.01, 0.01]$.

Several test-cases were performed in order to assess the properties of the method. The results are shown in Table 3.1, when the number of points N_P and the number of modes N_M is varied. As expected, the results show a monotonic behavior. At fixed number of modes, the error decreases when the number of collocation points are increased, and the speed-up decreases. Similarly, by keeping fix the number of points, the error decreases when the number of modes are increased, and the speed-up decreases. Remark that the speed-up obtained is significant, being of about two orders of magnitude.

In Figure 3.1 we compare the FE solution (left) with the ALP-EI method for $N_m = 15$, $N_p = 50$ (middle) and we show the relative error (right)

$$\mathrm{error}(t^n) = \frac{|v_{\mathrm{m}}(t^n) - \hat{\mathbf{\Phi}}(t^n)\beta(t^n)|}{max|v_{\mathrm{m}}(t^n)|} \tag{3.7}$$

for different time-steps. We see that the results are satisfactory with a very low number of modes and interpolation points.

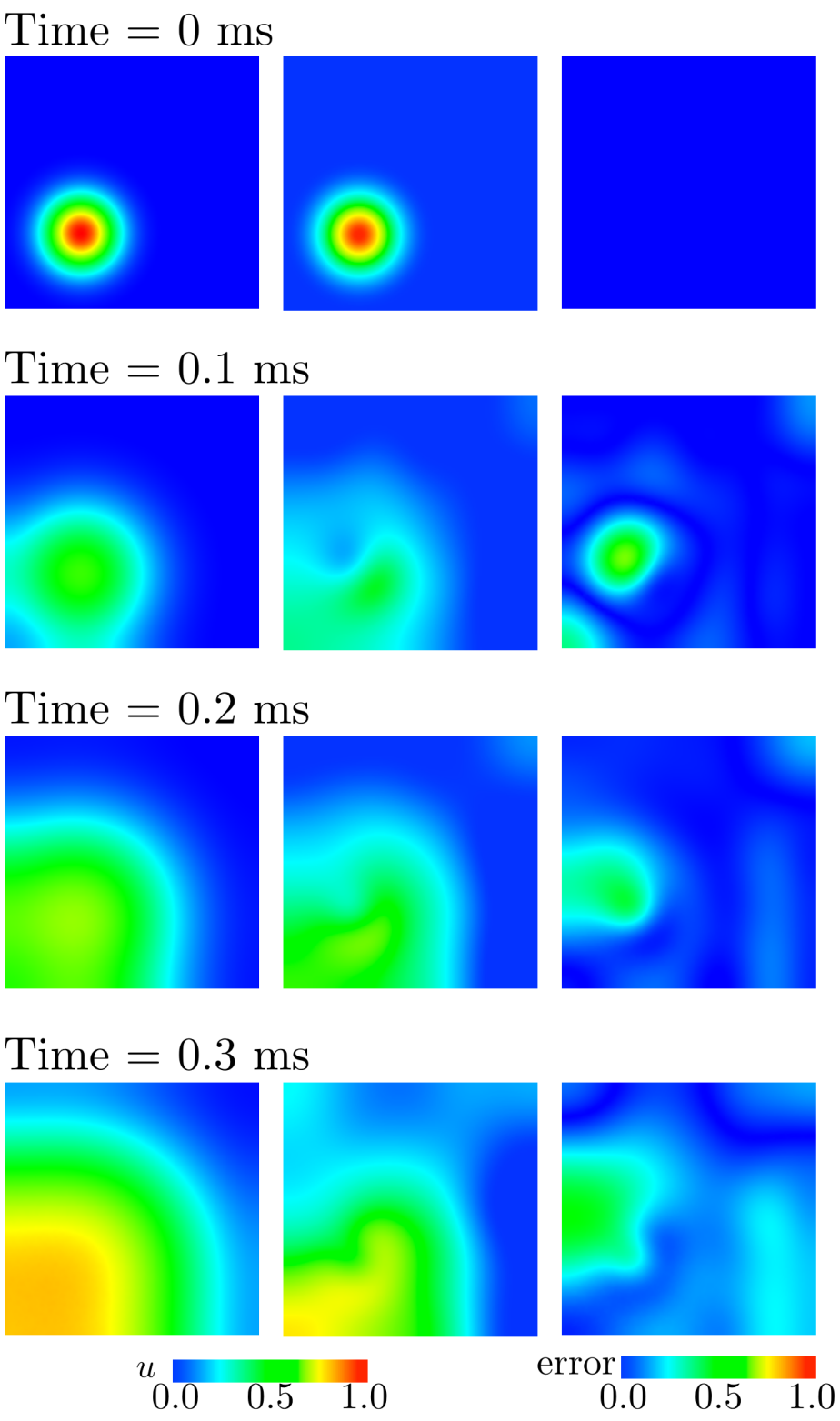

FIG. 3.1. *2D test case for problem (3.1). FEM solution (left), ALP-EI solution with $N_m = 15$, $N_p = 50$ (middle) and relative error (right).*

N_{M}	N_{P}	$\|e\|_{l^2(l^2)}$	time per iter. (msec)	speed-up
25	101	1.81×10^{-2}	1.3674	184
	150	1.69×10^{-2}	3.1339	80
	200	1.27×10^{-2}	6.2504	40
30	101	1.68×10^{-2}	1.7445	144
	150	1.67×10^{-2}	3.8966	64
	200	1.24×10^{-2}	7.4561	34
35	101	1.50×10^{-2}	2.1159	119
	150	1.48×10^{-2}	4.7405	53
	200	1.12×10^{-2}	9.0164	28
40	101	1.48×10^{-2}	2.5028	100
	150	1.44×10^{-2}	5.6005	45
	200	1.10×10^{-2}	10.7833	23

TABLE 3.1

Relative error in $l^2(l^2)$ norm, time per iteration and speed-up compared to FEM (5k dof, time per iteration = 251.3866 msec) varying number of modes (from 25 to 50) and number of points (from 101 to 200) for FKPP equation.

3.2. Cardiac electrophysiology. We are now interested in applying the ALP-EI method to some non-polynomial nonlinear test cases. Let us concentrate on the so-called *monodomain* equations [4] used to describe the electrical potential in a cardiac tissue. Monodomain equations are a simplified version of the *bidomain* equations [14]. Even if in some cases, such as for electrocardiogram or defibrillation simulation [2], bidomain equations are needed, in many cases monodomain equations prove to be sufficient [4].

In their general formulation, monodomain equations read

$$\left\{ \begin{array}{rcl} A_{\mathrm{m}}\Big(C_{\mathrm{m}}\dfrac{\partial v_{\mathrm{m}}}{\partial t} + I_{\mathrm{ion}}(v_{\mathrm{m}}, w)\Big) - \mathrm{div}(\boldsymbol{\sigma}_{\mathrm{i}}\nabla v_{\mathrm{m}}) & = & A_{\mathrm{m}} I_{\mathrm{app}}(x,t), \\ \dfrac{\partial w}{\partial t} - g(v_{\mathrm{m}}, w) & = & 0, \end{array} \right. \tag{3.8}$$

with the following boundary conditions on $\partial\Omega$

$$\left\{ \boldsymbol{\sigma}_{\mathrm{i}}\nabla v_{\mathrm{m}} \cdot \mathbf{n} = 0, \right. \tag{3.9}$$

where v_{m} represents the transmembrane potential, A_{m} and C_{m} are the ratio of membrane area per unit volume and the membrane capacitance per area respectively, $\boldsymbol{\sigma}_{\mathrm{i}}$ denotes the intra-cellular conductivity tensor (see for instance [12]) and I_{app} is a given source term. The nonlinear reaction term $I_{\mathrm{ion}}(v_{\mathrm{m}}, w)$ representing a ionic current is given by the solution of an ODE system. In what follows we consider the Mitchell and Schaeffer ionic model [10]

$$\begin{aligned} I_{\mathrm{ion}}(v_{\mathrm{m}}, w) &= w\frac{v_{\mathrm{m}}^2(1-v_{\mathrm{m}})}{\tau_{\mathrm{in}}} + \frac{v_{\mathrm{m}}}{\tau_{\mathrm{out}}}, \\ g(v_{\mathrm{m}}, w) &= \left\{ \begin{array}{ll} \dfrac{w-1}{\tau_{\mathrm{open}}}, & v_{\mathrm{m}} < v_{\mathrm{gate}}, \\ \dfrac{w}{\tau_{\mathrm{close}}}, & v_{\mathrm{m}} > v_{\mathrm{gate}}, \end{array} \right. \end{aligned} \tag{3.10}$$

where τ_{in}, τ_{out}, τ_{open}, τ_{close}, v_{gate} are scalar parameters.

In order to apply the ALP-EI method, we follow the same steps given in the previous example. To take into account anisotropic $\boldsymbol{\sigma}_\mathrm{i}$ due to the presence of fibers in the cardiac tissue, we define the spectral operator used to compute the initial basis as

$$\mathcal{L}(u)\varphi = -\mathrm{div}(\boldsymbol{\sigma}_\mathrm{i}\nabla\varphi) - \chi u\varphi, \tag{3.11}$$

where the solution u is the transmembrane potential v_m.

Then we approximate the transmembrane potential v_m by $v_\mathrm{m} \simeq \sum \beta_i\varphi_i$, and consider problem (3.8) approximated on the first N_M modes:

$$A_\mathrm{m}C_\mathrm{m}\sum_{i=1}^{N_M}\partial_t\beta_i\varphi_i + \beta_i\partial_t\varphi_i - \sum_{i=1}^{N_M}\beta_i\mathrm{div}(\boldsymbol{\sigma}_\mathrm{i}\nabla\varphi_i) = -A_\mathrm{m}(I_\mathrm{ion}(v_\mathrm{m},w) - I_\mathrm{app}) \tag{3.12}$$

Using $-\mathrm{div}(\boldsymbol{\sigma}_\mathrm{i}\nabla\varphi_i)\varphi_i = \chi v_\mathrm{m}\varphi_i + \lambda_i\varphi_i$ in this relation:

$$A_\mathrm{m}C_\mathrm{m}\sum_{i=1}^{N_M}\partial_t\beta_i\varphi_i + \beta_i\partial_t\varphi_i - \sum_{i=1}^{N_M}\beta_i(\chi v_\mathrm{m}\varphi_i + \lambda_i\varphi_i) = -A_\mathrm{m}(I_\mathrm{ion}(v_\mathrm{m},w) - I_\mathrm{app}). \tag{3.13}$$

After some algebra and by noticing that $\sum_i \beta_i v_\mathrm{m}\varphi_i = v_\mathrm{m}^2$, the expression becomes:

$$A_\mathrm{m}C_\mathrm{m}\sum_{i=1}^{N_M}\partial_t\beta_i\varphi_i + \beta_i\partial_t\varphi_i = -A_\mathrm{m}(I_\mathrm{ion}(v_\mathrm{m},w) - I_\mathrm{app}) - \chi v_\mathrm{m}^2 - \sum_{i=1}^{N_M}\beta_i\lambda_i\varphi_i. \tag{3.14}$$

This equation is discretised on the N_P points and the equations for the coefficients $\hat{\beta}$ is found by projecting the equation on the basis:

$$A_\mathrm{m}C_\mathrm{m}(\partial_t\hat{\beta} + M\hat{\beta}) = -A_\mathrm{m}\langle(I_\mathrm{ion}(\hat{v_\mathrm{m}},\hat{w}) - I_\mathrm{app}), \hat{\boldsymbol{\Phi}}\rangle + -\chi\langle\hat{v_\mathrm{m}}^2, \hat{\boldsymbol{\Phi}}\rangle + \Lambda\hat{\beta}. \tag{3.15}$$

Remark that the nonlinear ODE system (3.10) is solved point-wise on the N_p points.

The full-order problem is defined on $\Omega = [0,1]^2$, discretised by a P_1 finite element, the number of degrees of freedom is $\mathcal{N} \approx 5\ 10^3$, a second order Backward Difference method is applied for the time discretization. Both full-order and reduced-order problems are discretized with a time step $\delta t = 0.01$ms. Parameters are taken as in Table 3.2.

First, we consider an homogeneous cardiac tissue on a 2D domain where a source term not included in the initial basis is introduced. Then, a spatial heterogeneity is introduced: the parameter that regulates the depolarization plateau duration is changed as in the cardiac tissue. It should be noted that with reduced-order methods like POD, this kind of test cases is difficult to handle without considering a huge amount of scenarios in the offline stage.

A_m	C_m	σ_i	τ_in	τ_out	τ_open	τ_close	v_gate
2000.0	0.1	1.0	4.0	50.0	100.0	80.0	0.13

TABLE 3.2
Bidomain equations and Mitchell and Schaeffer ionic model parameters.

Source terms. First, we consider the monodomain equations with the Mitchell and Schaeffer model, without fiber tensors orientation and with homogeneous parameters. The challenging point is the treatment of the non-polynomial term in the Mitchell and Schaeffer ionic model.

The initial basis is computed using the FE solution at time $t = 5$ms, with $\chi = 25$, and the solution is run with $N_{\mathrm{M}} = 25$ basis modes. In Figure 3.2 the results with the ALP-EI method (middle) are compared to the FE ones (left). We can see that the reduced order solution is very close to the FE element solution. This can also be observed in the relative error in Figure 3.2 right. The error is less than 10% for most of the time except at about 25ms when the propagation front "exits" the domain, but in all cases it does not exceed 30%.

Then, a source term located in a different position compared to the first one is applied. After the end of the complete cardiac cycle and whole reporazitation of the tissue, the second applied stimulus is located in the top-left corner of the domain as shown in Figure 3.3 (first row). The application of a new source term is particularly simple in the framework of the ALP-EI algorithm.

The results in Figure 3.3 show a good agreement between the FE and the reduced-order solutions, which is run with $\chi = 25$ and $N_{\mathrm{M}} = 25$ modes. The error presents some oscillations at the moment of the source term application, probably due to the change of direction of the first modes of the basis, but it is in general of very low values, at most less than 10%.

Several tests are run with different number of modes N_m and of points N_p. Results are schematized in Table 3.3. We can observe that satisfactory results both in term of relative error, wich is limited to 10^{-2} for small values of N_m and N_p, and of speed-up of the method.

Heterogeneous ionic parameters. We are now interested in introducing some heterogeneities in the ionic parameters. In particular, we reproduce the cardiac tissue heterogeneity by considering three different cell types: endocardial, mid-myocardial and epicardial cells. The parameter τ_{close} of the ionic model varies in these three layers illustrated in Figure 3.4 top-left, and takes values given in Table 3.4. Owing to this heterogeneity, the solution has a repolarization front which propagates in the opposite direction to the depolarization one.

The ROM simulation is run with $N_{\mathrm{M}} = 25$ modes and $\chi = 25$, and the initial basis is computed from the FE solution at time $t = 5$ms. We can see in Figure 3.4 that the reduced-order solution (middle) is very close to the FE one (left) both in the depolarization phase (second row) and in the repolarization one (third row), and the error takes locally values of at most 30% and does not exceed 5% elsewhere.

Also in this case, several tests varying the number of modes N_m and the number of points N_p are run. Results of Table 3.5 show satisfactory behavior of the method both in terms of relative error and speed-up of the resolution.

4. Improved approximation of the eigenmodes evolution. During our numerical tests, we observed that, in some situations, it may be useful to use an improved approximation of the time evolution of the eigenmodes. In this Section, we present a strategy to do so, and we illustrate it on a simple linear advection equation.

4.1. Basis dynamics. The basis time derivative can be approximated as the sum of an endomorphism and a linear transformation defined in the space orthogonal to the space spanned by the modes. In particular, let us define R the matrix of the

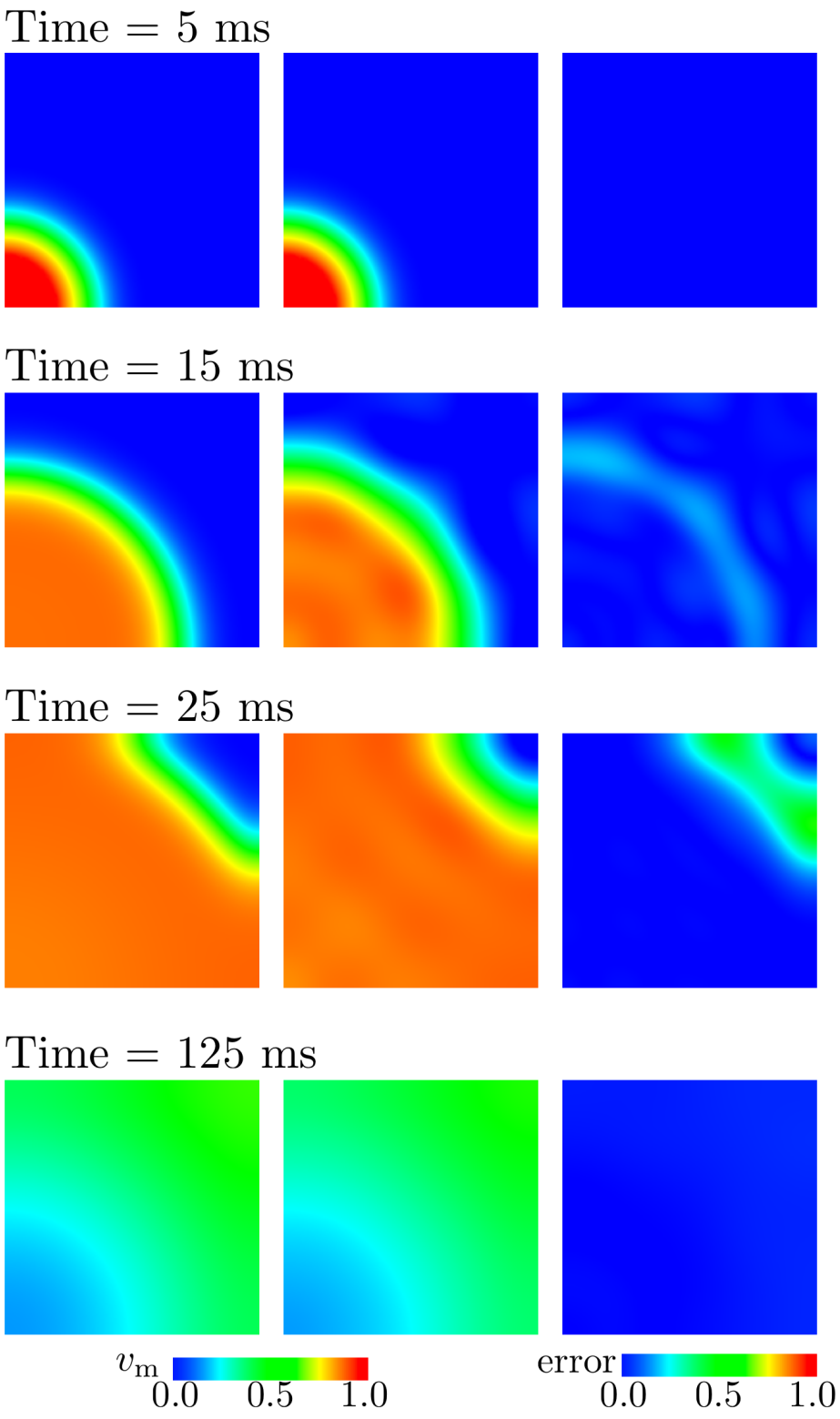

FIG. 3.2. *2D test case with homogeneous parameters. FEM solution (left), ALP-EI solution (middle) and relative error (right).*

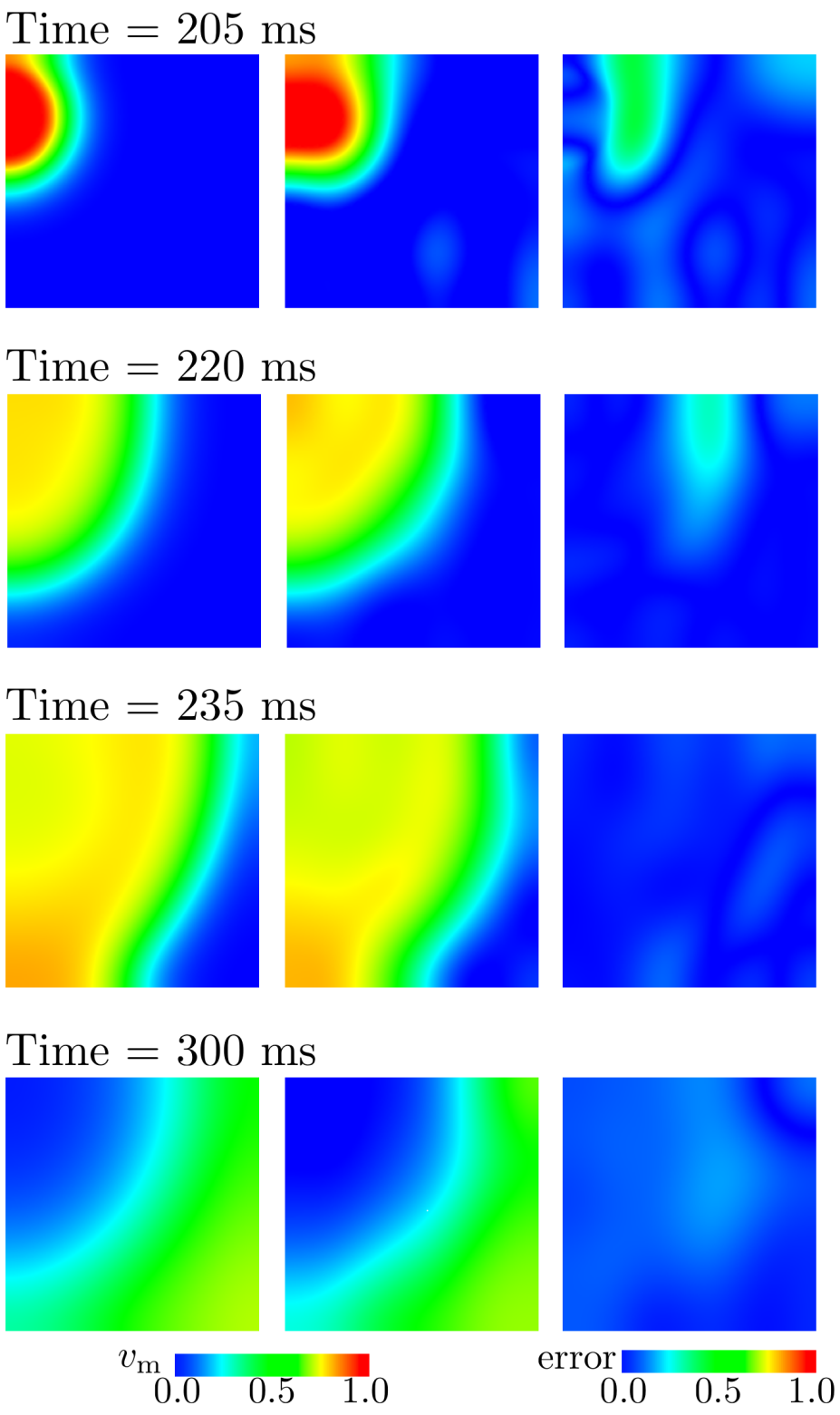

FIG. 3.3. *2D test case with source term. FEM solution (left), ALP-EI solution (middle) and relative error (right).*

N_{M}	N_{P}	$\|e\|_{l^2(l^2)}$	time per iter. (msec)	speed-up
	26	2.52×10^{-2}	0.0892	330
	30	2.44×10^{-2}	0.1050	280
10	41	2.75×10^{-2}	0.1521	193
	50	2.83×10^{-2}	0.1990	147
	62	3.12×10^{-2}	0.2723	108
	26	1.41×10^{-2}	0.1583	185
	30	1.81×10^{-2}	0.1845	159
15	41	2.28×10^{-2}	0.2683	109
	50	2.16×10^{-2}	0.3454	85
	62	2.81×10^{-2}	0.4692	62
	26	1.32×10^{-1}	0.2735	107
	30	5.28×10^{-2}	0.3169	92
21	41	1.80×10^{-2}	0.4515	65
	50	1.50×10^{-2}	0.5757	51
	62	2.47×10^{-2}	0.7624	38
	26	2.20×10^{-1}	0.3754	78
25	41	2.19×10^{-2}	0.6050	48
	50	1.24×10^{-2}	0.7606	38
	62	2.39×10^{-2}	0.9960	29
	30	2.14×10^{-1}	0.5989	49
30	41	1.77×10^{-2}	0.8244	35
	50	1.27×10^{-2}	1.0421	28
	62	2.39×10^{-2}	1.3311	22

TABLE 3.3

Relative error in $l^2(l^2)$ norm, time per iteration and speed-up compared to FEM (5k dof, time per iteration = 29.4410 msec) varying number of modes (from 10 to 30) and number of points (from 26 to 62) for monodomain equation with a source term.

$\tau_{\mathrm{close}}^{\mathrm{endo}}$	$\tau_{\mathrm{close}}^{\mathrm{Mcell}}$	$\tau_{\mathrm{close}}^{\mathrm{epi}}$
90.0	70.0	50.0

TABLE 3.4

Ionic parameters for heart model.

residual in the basis evolution equation:

$$\partial_t \Phi = \Phi M + R, \tag{4.1}$$

where R is orthogonal to the space spanned by the modes and M is the representation of $\mathcal{M}$ on the basis.

In order to practically compute R in an efficient way, the above identity is specialised for the collocation space of size N_{P}, that is in a bijection with the space spanned by N_{P} modes at the initial time. An orthogonal basis, *i.e.* a basis of the orthogonal complement to $\hat{\Phi}$, is defined as

$$\Phi^{\perp} = [\Psi_{N_M+1} \cdots \Psi_{N_P}] - \hat{\Phi}\hat{\Phi}^T G[\Psi_{N_M+1} \cdots \Psi_{N_P}], \tag{4.2}$$

where Ψ_i is the i-th column of Ψ. Only few elements of Ψ are retrieved, let us call the dimension of $\Phi^{\perp}$ $N^{\perp} \leq N_{\mathrm{P}} - N_{\mathrm{M}}$. The partial derivatives of the modes is

N_{M}	N_{P}	$\|e\|_{l^2(l^2)}$	time per iter. (msec)	speed-up
10	26	4.55×10^{-2}	0.0852	374
	30	4.60×10^{-2}	0.1022	311
	41	4.36×10^{-2}	0.1482	215
	50	4.41×10^{-2}	0.1962	162
	62	4.36×10^{-2}	0.2699	118
15	26	4.27×10^{-2}	0.1541	206
	30	4.28×10^{-2}	0.1778	179
	41	4.21×10^{-2}	0.2605	122
	50	4.21×10^{-2}	0.3360	94
	62	4.15×10^{-2}	0.4636	68
21	26	4.06×10^{-2}	0.2604	122
	30	4.32×10^{-2}	0.3090	103
	41	4.07×10^{-2}	0.4338	73
	50	4.05×10^{-2}	0.5611	56
	62	4.02×10^{-2}	0.7566	42
25	26	1.08×10^{-2}	0.3517	90
	30	1.92×10^{-2}	0.4078	78
	41	1.74×10^{-2}	0.5779	55
	50	1.30×10^{-2}	0.7409	43
	62	1.31×10^{-2}	0.9928	32
30	30	3.94×10^{-2}	0.5657	56
	41	3.91×10^{-2}	0.7900	40
	50	3.94×10^{-2}	1.0106	31
	62	3.94×10^{-2}	1.3259	24

TABLE 3.5

Relative error in $l^2(l^2)$ norm, time per iteration and speed-up compared to FEM (5k dof, time per iteration = 31.8843 msec) varying number of modes (from 10 to 30) and number of points (from 26 to 62) for monodomain equation with heterogeneout τ_{close} parameter.

approximated by

$$\partial_t \hat{\Phi} \simeq \hat{\Phi} M + \Phi^{\perp} C, \tag{4.3}$$

and this expression is injected into equation (2.12), leading to

$$G\hat{\Phi}\Lambda M + L\Phi^{\perp} C - G\hat{\Phi} M\Lambda - G\Phi^{\perp} C\Lambda = G\hat{\Phi}\dot{\Lambda} + \chi G\partial_t \hat{u} \odot \hat{\Phi}. \tag{4.4}$$

The projection of this equation onto Φ has already been computed and leads to the representation of the evolution operator and the time derivative of the eigenvalues, since $\Phi^{\perp}$ is by construction orthogonal to Φ. The projection onto $\Phi^{\perp}$ allows us to determine the expression of C:

$$(\Phi^{\perp})^T L\Phi^{\perp} C - (\Phi^{\perp})^T G\Phi^{\perp} C\Lambda = \chi(\Phi^{\perp})^T G\partial_t \hat{u} \odot \hat{\Phi}. \tag{4.5}$$

Thus, a matrix equation for C can be written for each mode separately. It can be demonstrated that the system matrix $(\Phi^{\perp})^T L\Phi^{\perp} - \lambda_i (\Phi^{\perp})^T G\Phi^{\perp}$, $i = 1, \ldots, N_{\mathrm{M}}$, for each mode is positive definite. If $\partial_t \hat{u} \odot \hat{\Phi}$ has a null projection in the space spanned by $\Phi^{\perp}$, C vanishes identically. Otherwise, the derivatives of the modes have a non-vanishing projection onto the orthogonal space if and only if the image of the

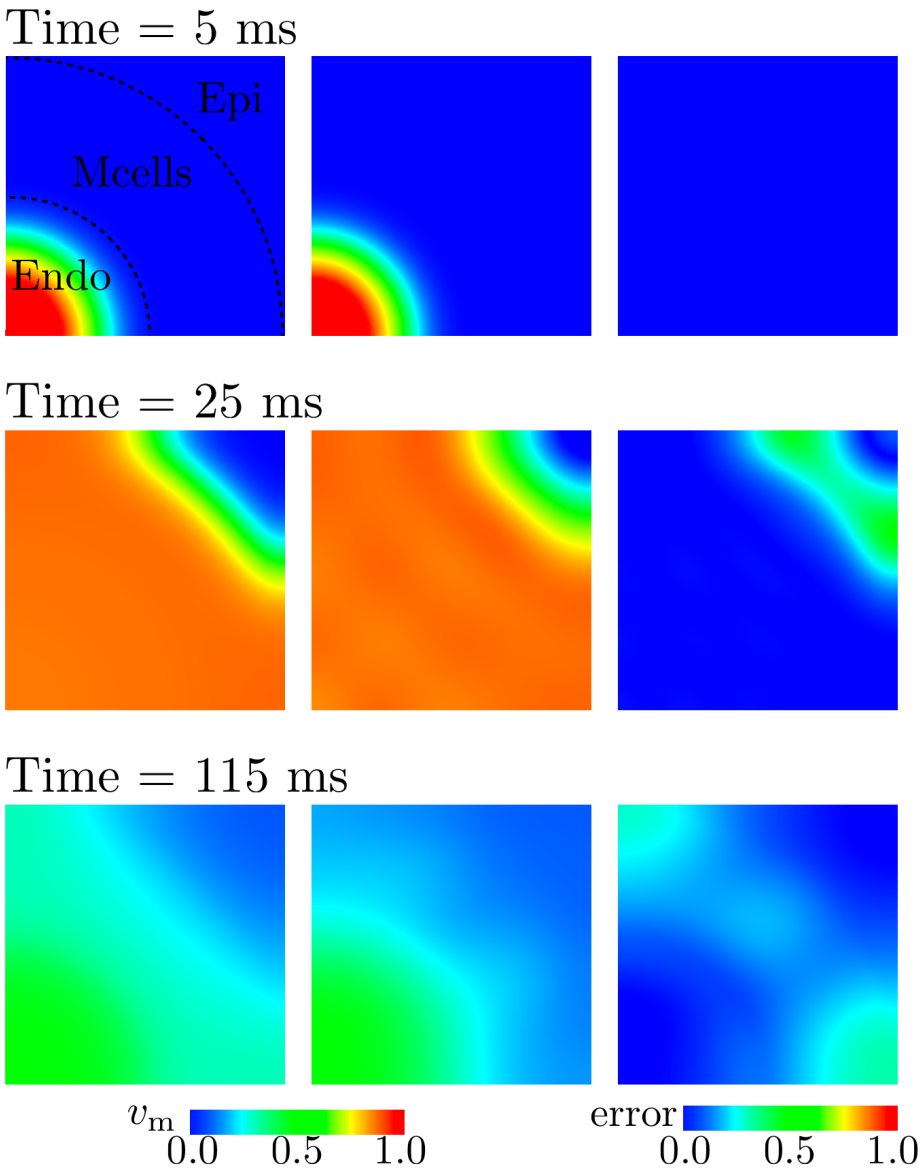

FIG. 3.4. *2D test case with heterogeneous parameter τ_{close}. FEM solution (left), ALP-EI solution (middle) and relative error (right).*

operator $\partial_t \hat{u} \odot \hat{\Phi}$ has. This, indeed, can be exploited to setup an *a posteriori* criterion to decide whether it is useful to compute the orthogonal complement part of the time derivative of the modes. The following simple numerical experiment on a linear advection equation provides a paradigmatic example of a situation in which the time derivative has a significant projection in the orthogonal complement of the basis.

4.2. Application: linear advection equation. To illustrate the construction explained in the previous section, we consider a linear advection equation in 1D on the

interval $\Omega = [0, 1]$. The main difference with respect to the parsimonious discretisation presented so far is that, for the linear advection problem, the operator ∂_x cannot be substituted by exploiting the spectral problem. For the present case, which provides also an example on how the proposed methodology can be extended to a broader class of problems, we decided to represent the operator ∂_x on the space spanned by the modes Ψ. The resulting matrix $D_x \in \mathbb{R}^{N_P \times N_p}$ is constructed as it is done in the spectral collocation approaches (see [13] for a comprehensive overview):

$$D_x \Psi = \mathcal{P}(\partial_x \Phi_0), \tag{4.6}$$

that is, the application of the matrix D_x to every collocated mode Ψ equals the collocation of the derivative performed in the full-order finite element space. This ensures that for every function belonging to the space spanned by Ψ the derivative has the same accuracy as that obtained in the full-order space.

An ALP-EI discretisation is performed by considering $N_P = 40$ points and $N_M = (10, 15, 20)$, $\Delta t = 5\ 10^{-3}$ and a Runge-Kutta impicit mid-point scheme in time. The exact solution is: $u = \exp(-250(x - 0.6t - 0.2)^2)$ for $t \in [0, 1]$. Two sets of experiments are performed, one in which the orthogonal complement part of the derivative is neglected and one in which it is taken into account. The results are

N_{M}	$\Phi^{\perp}$	$\|e\|_{l^2(l^2)}$
10	no	0.3119
10	yes	0.0472
15	no	0.0851
15	yes	0.0195
20	no	0.0219
20	yes	0.0137

TABLE 4.1

Relative $\ell_2(\ell_2)$ error on the evolution of a linear advection equation when $N_P = 40$, $N_M = (10, 15, 20)$ when the projection onto the orthogonal complement of the basis is considered and when it is neglected.

reported in Table 4.1. The difference between the results obtained by considering and by neglecting the projection of the derivative of the modes on the orthogonal complement is very significant, especially when the number of modes is low.

REFERENCES

[1] M. Barrault, Y. Maday, N. C. Nguyen, and A. T. Patera. An "empirical interpolation" method: Application to efficient reduced-basis discretization of partial differential equations. *C. R. Math. Acad. Sci. Paris*, 339:667–672, 2004.

[2] M. Boulakia, S. Cazeau, M.A. Fernández, J-F. Gerbeau, and N. Zemzemi. Mathematical modeling of electrocardiograms: a numerical study. *Annals of Biomedical Engineering*, 38(3):1071–1097, 2010.

[3] S. Chaturantabut and D. Sorensen. Nonlinear model reduction via discrete empirical interpolation. *SIAM Journal of Scientific Computing*, 32(5):2737–2764, 2010.

[4] P. Colli Franzone, L.F. Pavarino, and B. Taccardi. Simulating patterns of excitation, repolarization and action potential duration with cardiac Bidomain and Monodomain models. *Mathematical Biosciences*, 197(1):35–66, 2005.

[5] P. Erdös. Problems and results on the theory of interpolation, II. *Acta Math. Acad. Sci.*, 12:235–244, 1961.

[6] J-F. Gerbeau and D. Lombardi. Approximated Lax Pairs for the Reduced Order Integration of Nonlinear Evolution Equations. *Journal of Computational Physics*, 265:246–269, 2014.

[7] J-F. Gerbeau, D. Lombardi, and E. Schenone. Reduced order model in cardiac electrophysiology with approximated Lax pairs. *Advances in Computational Mathematics*, 41(5):1103–1130, 2015.

[8] M. A. Grepl, Y. Maday, N. C. Nguyen, and A. T. Patera. Efficient reduced-basis treatment of nonaffine and nonlinear partial differential equation. *ESAIM: Mathematical Modelling and Numerical Analysis*, 41(3):575–605, 2007.

[9] P. D. Lax. Integrals of nonlinear equations of evolution and solitary waves. *Comm. Pure Appl. Math.*, 21:467–490, 1968.

[10] C.C. Mitchell and D.G. Schaeffer. A two-current model for the dynamics of cardiac membrane. *Bulletin Math. Bio.*, 65:767–793, 2003.

[11] T. J. Rivlin. *An introduction to the approximation of functions*. Dover Publications Inc., New York, 1981.

[12] D.D. Streeter. Gross morphology and fiber geometry of the heart. *Handbook Physiology, The cardiovascular system*, 1:61–112, 1979.

[13] Lloyd N Trefethen. *Spectral methods in MATLAB*, volume 10. Siam, 2000.

[14] L. Tung. *A bi-domain model for describing ischemic myocardial d-c potentials*. PhD thesis, Massachusetts Institute of Technology. Dept. of Electrical Engineering and Computer Science, 1978.